Exploring Alloy Design Pathway Through Directed Energy Deposition of Powder Mixtures: A Study of Stainless Steel 316L and Inconel 718

Noah Sargent⁺, Yuankang Wang⁺, Daozheng Li, Yunhao Zhao, Xin Wang, Wei Xiong^{*}

Physical Metallurgy and Materials Design Laboratory,

Department of Mechanical Engineering and Materials Science,

University of Pittsburgh, PA 15261, USA

* Corresponding author: Email: weixiong@pitt.edu; URL: https://sites.pitt.edu/~weixiong

+ Both authors made equal contributions to this work.

Abstract

Additive manufacturing (AM) is a tool for rapid prototyping with complex geometry. However, the cyclic

heating and cooling in laser melting processes often cause large columnar grains that dominate the as-

printed microstructure, resulting in a strong texture and anisotropic properties that limit the application of

AM. In this work, we apply powder-based directed energy deposition to discover new alloys using mixtures

of Inconel 718 (IN718) and Stainless Steel 316L (SS316L). We discovered that the 77 wt.% IN718 alloy

mixture, with the highest configurational entropy, demonstrated an intriguingly fine grain structure in the

as-built condition and after homogenization at 1180°C. Residual stress from the laser melting process was

identified as the primary cause of the observed grain refinement phenomenon. Although, a quantitative

analysis of the changes in grain size after homogenization in the alloy mixtures of IN718 and SS316L

requires further research. The discovery of this unique microstructural behavior shows how in-situ mixing

of commercially available powders can be used to develop next-generation feedstock materials for AM and

improve the understanding of fundamental process-microstructure-property relationships.

Keywords: Directed energy deposition, entropy, grain refinement, alloy design

1

1. Introduction

Laser-based additive manufacturing (AM) is a promising prototyping technique because net shape components with complex geometries can be easily fabricated using sliced 3D models [1, 2]. However, many AM processes introduce anisotropy in microstructure and properties due to the unique cyclic melting process with a high thermal gradient [3]. For example, strong grain texture along the build direction in asprinted Inconel 718 (IN718) requires post-heat treatment to reduce directional differences in mechanical strength [4, 5]. Unlike traditional manufacturing methods, thermomechanical processes, such as forging and cold rolling, are avoided to maintain the geometric integrity of AM components. Therefore, identifying effective post-processing steps that eliminate grain texture, residual stress, and segregation while introducing grain refinement is highly desirable.

Directed energy deposition (DED) can mix multiple feedstock materials together to produce new alloy compositions [6] and composition gradients known as functionally graded materials [7-9]. This unique manufacturing capability is a useful rapid processing method for high-throughput alloy development [10]. Welk et al. [11] mixed a bulk metallic glass with a high entropy alloy to investigate the glass-forming ability of novel alloy mixtures. Kong et al. [12] used dual feed additive manufacturing to investigate the effect of Nb concentration on the microstructure and mechanical properties of IN718 by mixing two IN718 feedstocks with different Nb content. Pegues et al. [13] mixed Ta, Nb, and T-6Al-4V with a transition metal HEA (CoCrFeMnNi) to investigate the effect of refractory elements on the properties of high entropy alloys. These works primarily focus on the as-built condition of the alloy mixtures or FGMs and do not investigate the impact of heat treatment on the microstructure and properties of the samples, except for the aging study by Kong et al. [12]. Future studies should extend their investigation of as-built alloy mixtures to include post-processed conditions.

It should be noted that, although starting from pure elemental feedstock is possible, it is rather challenging to manufacture components with the desired composition, especially when alloying elements are required at very low concentration levels [14-17]. Additionally, purchasing feedstock powder with custom compositions typically costs much more than established off-the-shelf alloys, and minimum order size requirements significantly increase the upfront cost and material waste during materials innovation. Qualification of new feedstock powders also requires significant effort with no guarantee the new alloy composition will be successful. Therefore, in-situ mixing of off-the-shelf feedstock materials using the DED process is a promising tool for discovering fundamental process-microstructure-property relationships and developing next-generation alloys for AM at a significantly reduced cost [13]. This work demonstrates that the DED method can effectively discover new alloy compositions by mixing available feedstock materials with good characteristic microstructure-property relationships. Such a methodology of using AM

for materials design will assist in expanding alloy inventory for cost-effective engineering applications with increased sustainability.

In this work, we demonstrate a pathway of alloy design and adaptation for AM through microstructure analysis of a functionally graded alloy from stainless steel 316L (SS316L) to superalloy IN718 manufactured using Laser Engineered Net Shaping (LENS®). IN718 is a widely used Ni-based superalloy with excellent high-temperature mechanical properties. SS316L is austenitic stainless steel that is used extensively in different engineering fields [18, 19]. Although these alloy powders are commercially available and have been studied extensively over the past decade [18-26], both alloys suffer from anisotropic properties caused by the columnar grain texture introduced during laser melting [5].

2. Experimental Design & Methods

As the starting point of this investigation, an attempt to manufacture a functionally graded material (FGM) from SS316L to IN718 has been made using the LENS® 450 system (Optomec, Inc., USA) [27, 28]. The as-built condition of the SS316L and IN718 FGM was analyzed with optical microscopy and electron backscatter diffraction as shown in Fig. 1 (a-d) [27, 28]. High-throughput characterization of the FGM from SS316L to IN718 revealed significant grain refinement within the 75 wt.% IN718 composition block as shown by the inverse pole figure maps in Fig. 1 (b) and (d). Using CALPHAD modeling, the alloy (total) and configurational entropy were calculated as a function of composition for all the possible mixtures of IN718 and SS316L. The configurational entropy, shown in Fig. 1(e), reaches a peak at 77 wt.% IN718 and corresponds well with the observed grain refinement in the 75 wt.% IN718 intermediate block within the FGM.

From this initial study, a correlation was observed between configurational entropy and grain refinement, prompting further investigation. It should be noted that the entropy debate in the high-entropy alloy (HEA) research community drove the model prediction of alloy entropy in this work [29, 30]. From a thermodynamic viewpoint, the total entropy is the intrinsic quality that determines the alloy behavior, while the configurational entropy is just one part of the mixing entropy term and is easy to calculate without using software such as Thermo-Calc [31]. As a consequence, both total and configurational entropy are calculated as a function of alloy composition (Fig. 1(e)) to guide the experimental design. According to the CALPHAD prediction using the Thermo-Calc TCNI11 database, the alloy with 62 wt.% IN718 has the highest value in total entropy, and the alloy with 77 wt.% IN718 has the highest value of configurational entropy. In addition, the alloy mixture with 47 wt.% IN718 shows the same total entropy as 77 wt.% IN718, although its configurational entropy is lower than 77 wt.% IN718.

Based on this analysis, three monolithic coupons with 47, 62, and 77 wt.% IN718 were manufactured using the Optomec LENS® 450 system to evaluate the impact of total entropy versus configurational entropy. **Figure 1(f)** illustrates the DED process used to manufacture the alloy mixtures studied in this work. Cubes with side lengths of 1 cm for each of the desired compositions were manufactured by calibrating the mass flow rate of two powder feedstocks.

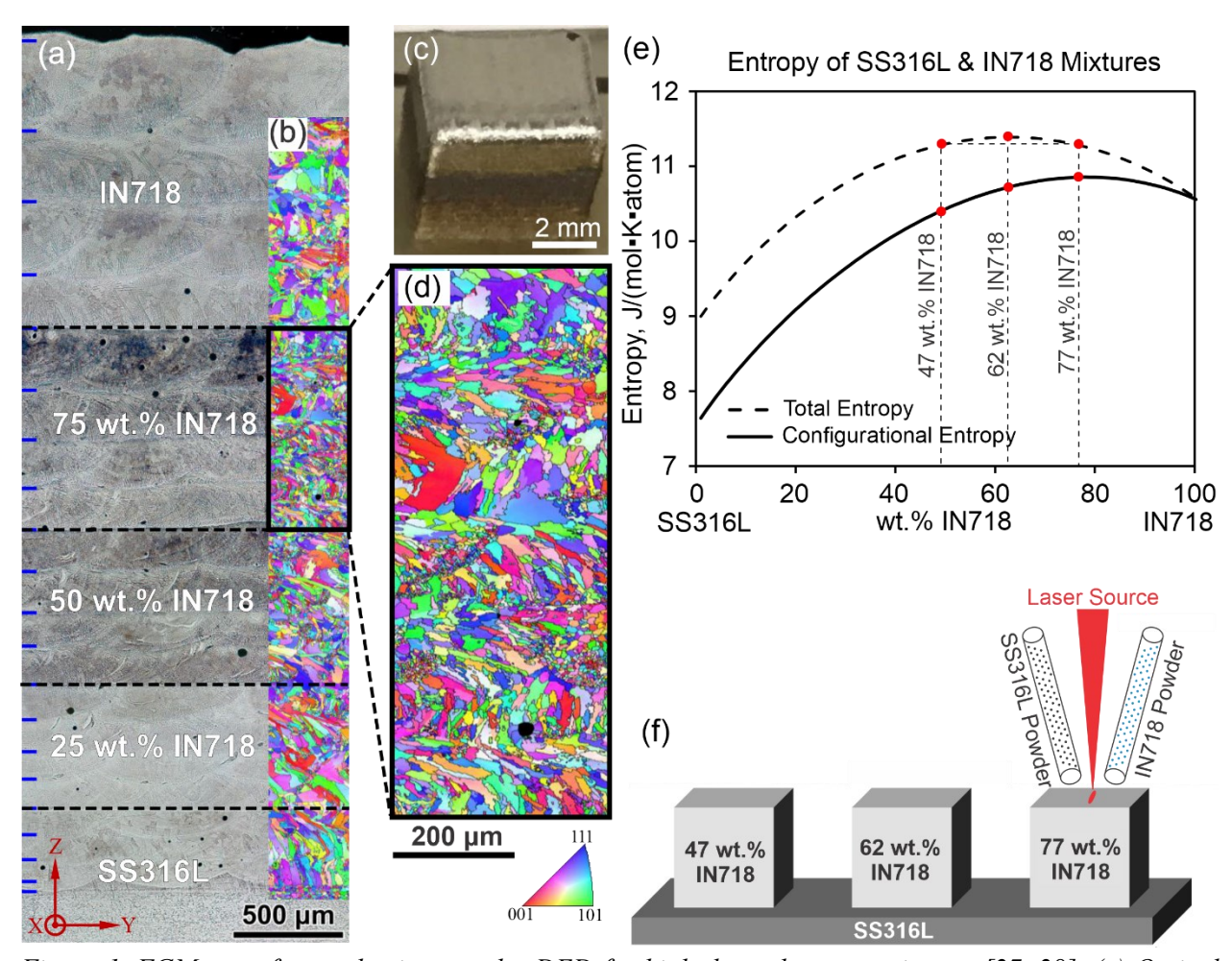


Figure 1. FGM manufactured using powder DED for high-throughput experiments [27, 28]. (a) Optical metallography of additively manufactured FGM from SS316L to IN718. (b) Inverse pole figure of grain texture. (c) Image of the IN718 and SS316L FGM before sectioning. (d) Magnified inverse pole figure of 75 wt.% IN718 and 25 wt.% SS316L composition block showing grain refinement. (e) Calculated configurational and total entropy of SS316L and IN718 mixtures. (f) Mixtures of SS316L and IN718 printed to study the effect of entropy on grain refinement.

All samples printed in this work share the same printing parameters. The printing process optimization was conducted based on the parameters used for pure SS316L and IN718. The optimized parameters are 300W laser power, 50 cm/min scanning speed, 0.381 cm hatch spacing, 0.25 cm layer height, mass flow rate of 6 g/min, 570 µm diameter spot size, and 38 cm/min contour scan speed. The SS316L powder is manufactured

by PRAXAIR with the composition of Fe-0.004C-1Mn-2Mo-17Cr-12Ni (wt.%), and the IN718 powder is from the same company with the composition of: Ni-0.04C-0.01Mn-2.93Mo-0.06Si-18.98Cr-0.41Al-0.94Ti-5.09Nb-18.15Fe (wt.%).

To evaluate the grain size and phase stability during post-heat treatment after laser melting, both as-built and homogenized samples were studied. After printing, the three alloy mixtures were subjected to high-temperature homogenization at 1180°C for 20 minutes, 1 hour, and 2 hours in an inert atmosphere, followed by ice water quenching. Microstructure analysis was performed using an SEM (FEI Apreo LoVac Analytical) equipped with an EBSD (electron backscatter diffraction) detector at an acceleration voltage of 20 kV and probe current of 13nA. It should be noted that the homogenization temperature is selected according to a comprehensive study performed by Zhao et al. [4] on the IN718 alloy made by AM.

3. Experimental and Computational Results

To better understand the phase stability and microstructure of the three alloy mixtures, the equilibrium step diagram (phase fraction vs. temperature) and Scheil solidification path have been predicted using the Thermo-Calc software with the TCNI11 database as shown in Fig. 2. The compositional accuracy of the printed samples was confirmed by comparing EDS measurements with the mixing ratio of the original feedstock powder compositions. This composition data is included in Table S7 in the supplementary materials. The Scheil modeling indicates that all three samples have two major phases, FCC (γ) and Laves, coexisting in the as-built microstructure. Both the Laves and y phases are observable in backscatter electron images of the as-built microstructures shown in Fig. 3(a-c). The Nb-rich Laves phase precipitates along the grain boundaries and in all three alloys. Due to the rapid heating/cooling process, the intermetallic compounds with low phase fractions, such as η and σ , predicted by the Scheil model are not observed. These findings are in good agreement with our previous experimental study on IN718 made by AM [4]. Although MC carbides are not observed in the as-built microstructure, after the dissolution of the Laves phase at 1180°C for 20min, a considerable amount of Nb-rich MC carbide forms inside the grains and along grain boundaries, as shown in Fig. 3(d-1). This is consistent with the equilibrium step diagram shown in Fig. 2(d-f), where the γ matrix and MC carbides are stable at 1180°C. Table S8 in the supplementary materials summarizes the measured volume fraction of MC carbide and Laves phases from the SEM images shown in Fig. 3. The phase fraction of Nb-rich MC carbide is low in all three alloys, with a slight increase of the MC phase fraction from the alloy with 47 wt.% IN718 to the one with 77 wt.% IN718.

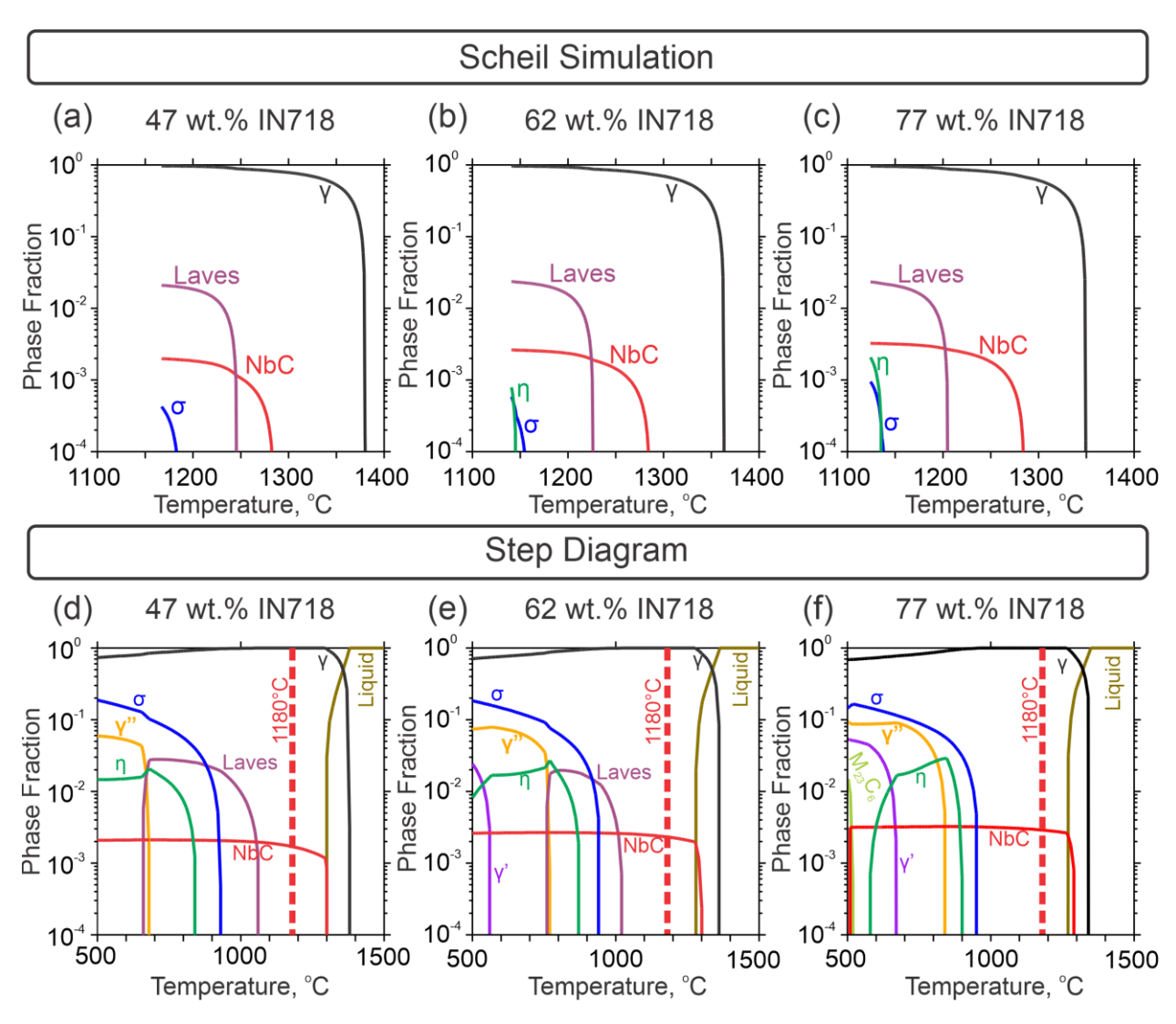


Figure 2. Step diagrams and Scheil solidification simulations of the SS316L and IN718 alloy mixtures. (a-c) Eon-equilibrium Scheil solidification modeling of 47, 62, and 77 wt.% IN718, respectively. (d-f) Equilibrium step diagrams of 47, 62, and 77 wt.% IN718, respectively.

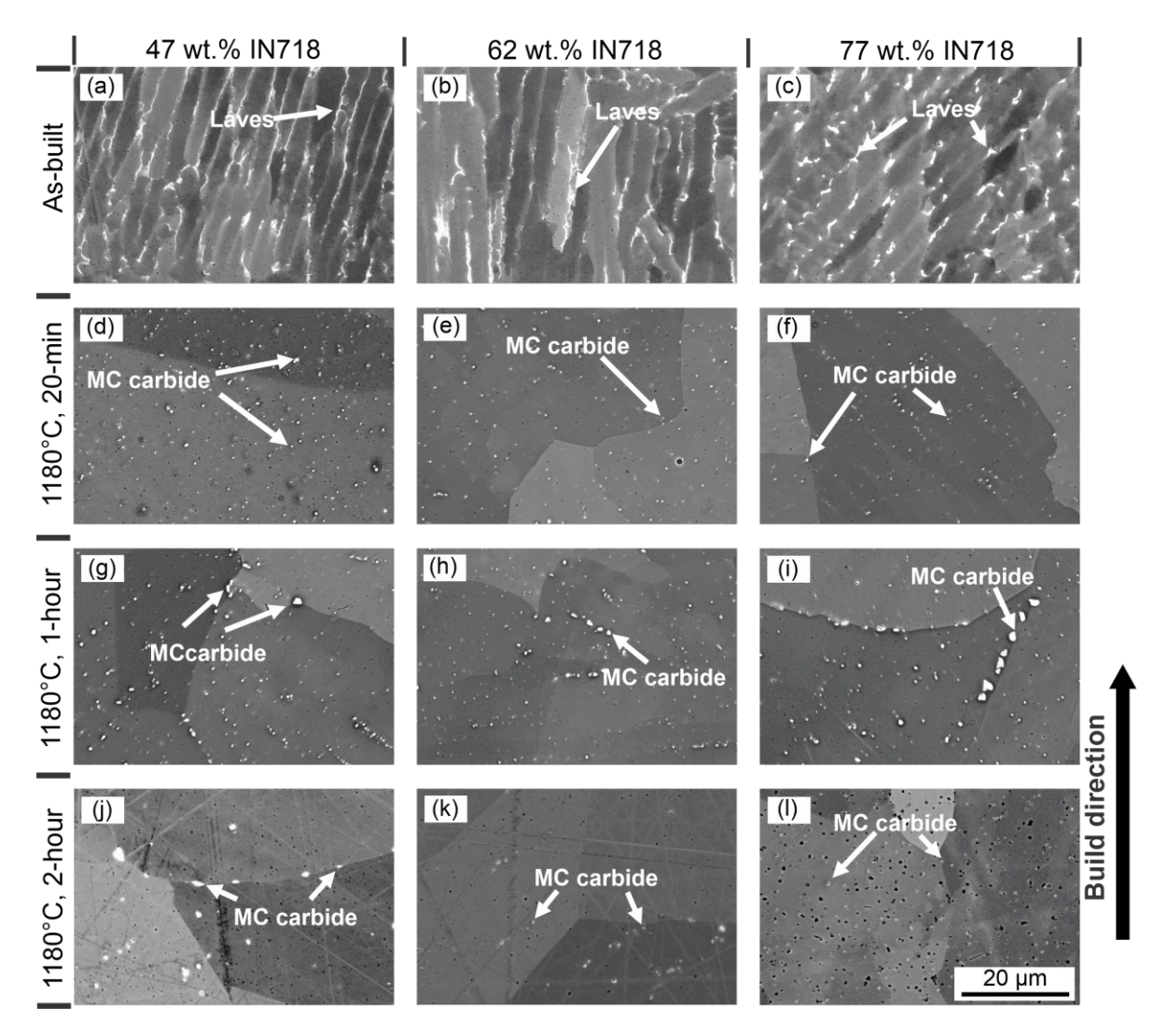


Figure 3. Microstructure of SS316L-IN718 alloy mixtures under SEM using backscatter electron imaging. (a-c) show the as-built condition. The samples after homogenization at 1180° C are presented in (d-f) for 20mins, (g-i) for 1 hour, and (j-l) for 2 hours. MC carbides are highly concentrated with Nb and can be considered as NbC. The scale bar shown in (l) can also be used for the other microstructure images.

IPF (Inverse Pole Figures) with a size of 1200 by 1200 μm were taken to determine the average grain size of the as-built and homogenized samples. **Fig. 4** compares the grain size of the as-built and homogenized samples as measured using EBSD. The as-built conditions of all three alloys have a columnar grain structure, and the average grain size is lowest in the alloy with 77 wt.% IN718 (85.5μm) when compared to the other alloys (106.2μm for 47 wt.% IN718 and 141.7μm for 62 wt.% IN718). Using the TSL OIM Analysis software developed by EDAX, Inc., the average grain size from each sample and condition is given in **Fig. S1(a)**. The aspect ratio calculated from the EBSD data is shown in **Fig. S1(b)**. Although the aspect ratio remains relatively the same after homogenization, the grain structure in the IPF maps appear less columnar, especially for the 77 wt.% IN718 sample homogenized for 1 hour. One possible explanation for this

discrepancy is that the formation of annealing twins during homogenization counteracts the removal of columnar grain texture and results in a constant aspect ratio.

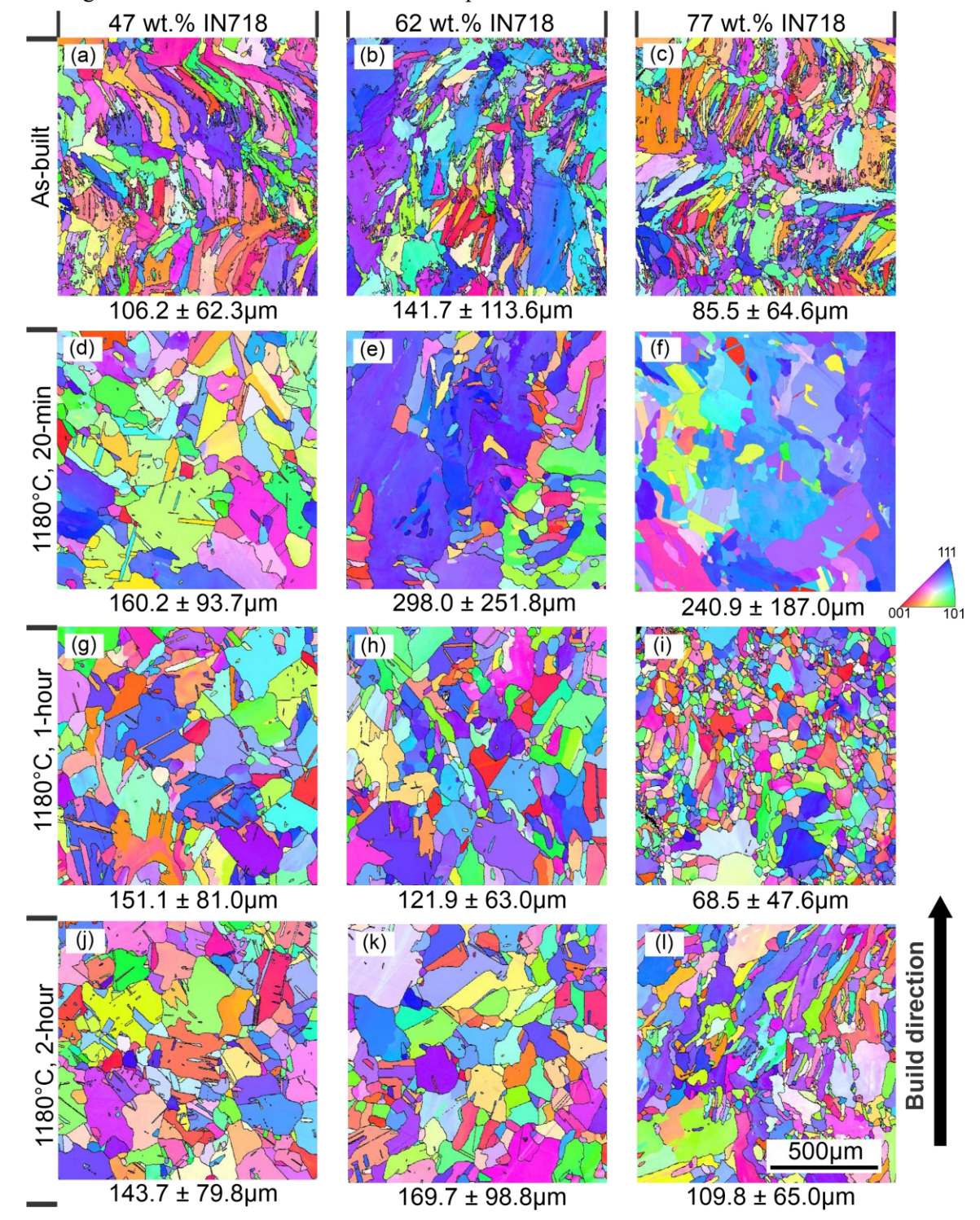


Figure 4. IPF maps of SS316L-IN718 mixed alloys. IPF maps of mixed alloys under (a-c) as-built condition, after homogenization at 1180°C for (d-f) 20 mins, (g-i) 1 hour, and (j-l) 2 hours. The average grain size and standard deviation of each IPF map are shown below the image. The scale bar shown in (l) can also be used for other the microstructure images.

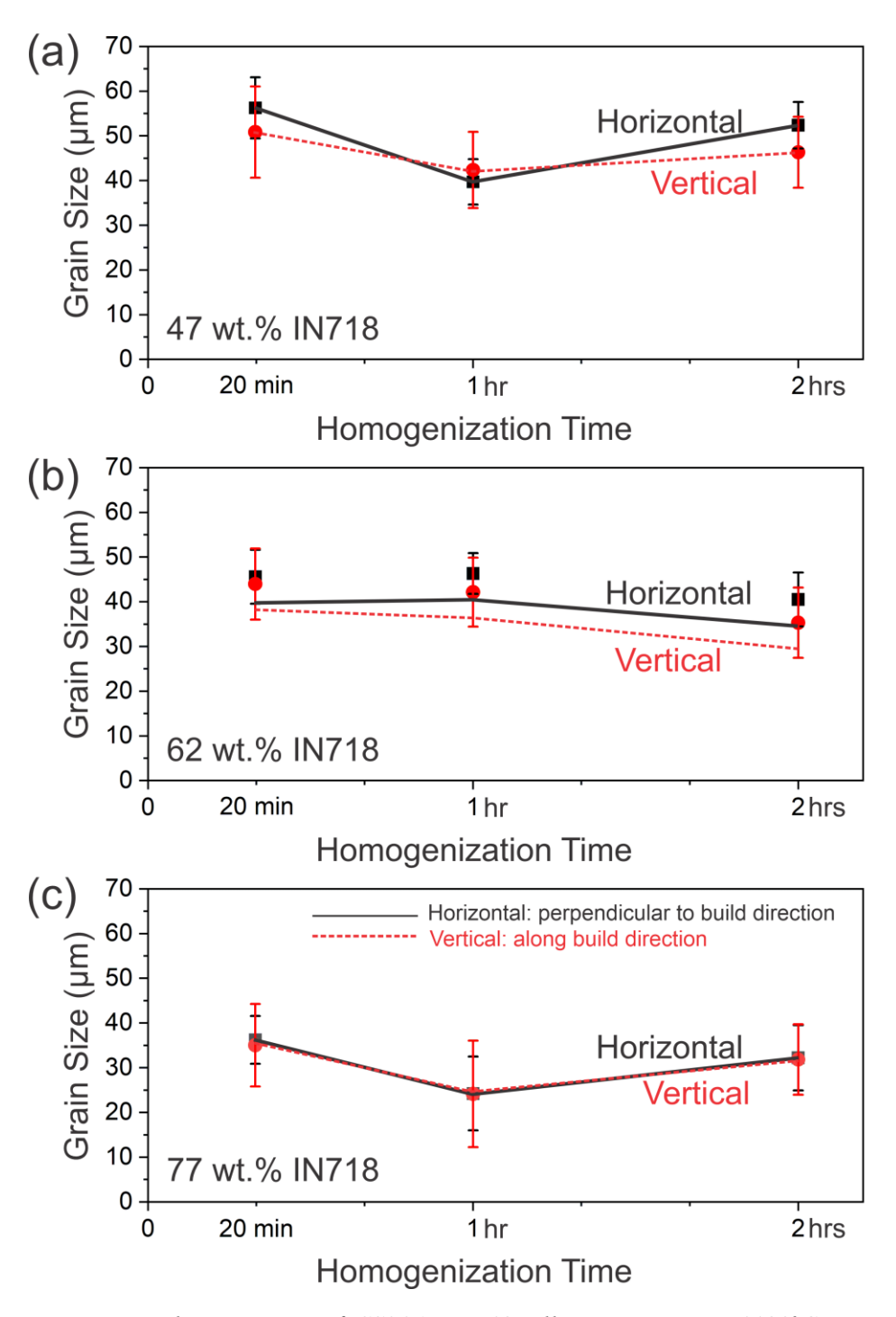


Figure 5. Directional grain size of SS316L-IN718 alloy mixtures at 1180°C as a function of homogenization time. Horizontal grain size is determined perpendicularly to the build direction according to the grain structure shown in the EBSD images in Figure 4. Vertical grain size is determined along the build direction. The grain size analysis was performed manually according to the intercept procedure of the ASTM standard E112.

The initial texture of the printed samples and the formation of annealing twins during homogenization causes a relatively considerable uncertainty in the standard deviation of the grain size. Therefore, a further dimensional grain size analysis was performed manually on the heat-treated condition according to the intercept procedure of the ASTM standard E112 (Standard Test Methods for Determining Average Grain Size). The horizontal grain size is determined perpendicularly to the build direction, while vertical grain size is along the build direction.

The most interesting takeaway from **Figs. 4 and 5** is that the grain size of all three alloys reaches a minimum after 1 hour of homogenization, and the alloy with 77 wt.% IN718 still has the smallest grain size. According to the analysis of the average grain size shown in **Fig. 5**, the sample with 77 wt.% IN718 after homogenization at 1180°C for 1 hour exhibits the finest average grain size of 68.5 µm. The significant grain refinement seen between the 20 min and 1-hour homogenization steps in all three alloys can be attributed to recrystallization. Such a grain refinement phenomenon is similar to the observation identified in IN718 superalloy prepared by LPBF (laser powder bed fusion) [4].

Grain orientation spread (GOS) maps were generated from the EBSD data and are shown in Fig. 6. GOS is considered in this work as a physical quantity to evaluate intergranular distortion and residual stress. Through the combined analysis of grain size and GOS, we gain valuable insights into the recrystallization process. Field et al. [32] pioneered the use of GOS for evaluating residual stress at the microstructural level. A similar comprehensive analysis has been performed by Zhao et al. [4] on IN718 made by LPBF. All three alloy mixtures exhibit the highest GOS values in the as-built condition, as shown in Fig. 6(a-c). High GOS levels in the as-built condition imply a high level of stored energy in the grains due to the residual stress generated through cyclic heating and cooling. After a 20-min homogenization, recrystallized grains are found in all three alloys, and the overall GOS value is reduced as shown in Fig. 6(d-f). In the alloy with 47 wt.% IN718, the GOS value reduces rapidly after only 20-min homogenization, implying the rapid consumption of stored energy. Most grains in the alloy with 47 wt.% IN718, after 20-min of homogenization, have a GOS value near zero. Although some localized areas show higher GOS values due to incomplete recrystallization. Since there is no obvious grain size change, it is reasonable to assume that recrystallization is mostly complete in less than 20-min for the alloy with 47 wt.% IN718. In the alloys with 62 and 77 wt.% IN718, there are several columnar grains with a high GOS value after 20-min homogenization, suggesting that the recrystallization process has not been completed. After 1-hour homogenization, both the 62 and 77 wt.% IN718 alloys undergo further grain refinement, particularly in the vicinity of grains with a high GOS value as shown in Fig. 6(i). Recrystallization is finished after 2-hour homogenization at 1180°C, and grain begins to grow further. Overall, the GOS in all three alloys steadily decreases with increasing homogenization time, indicating that the stored energy due to the residual stress

from the printing process has been dissipated. Among the three alloys, the GOS of the alloy with 77 wt.%

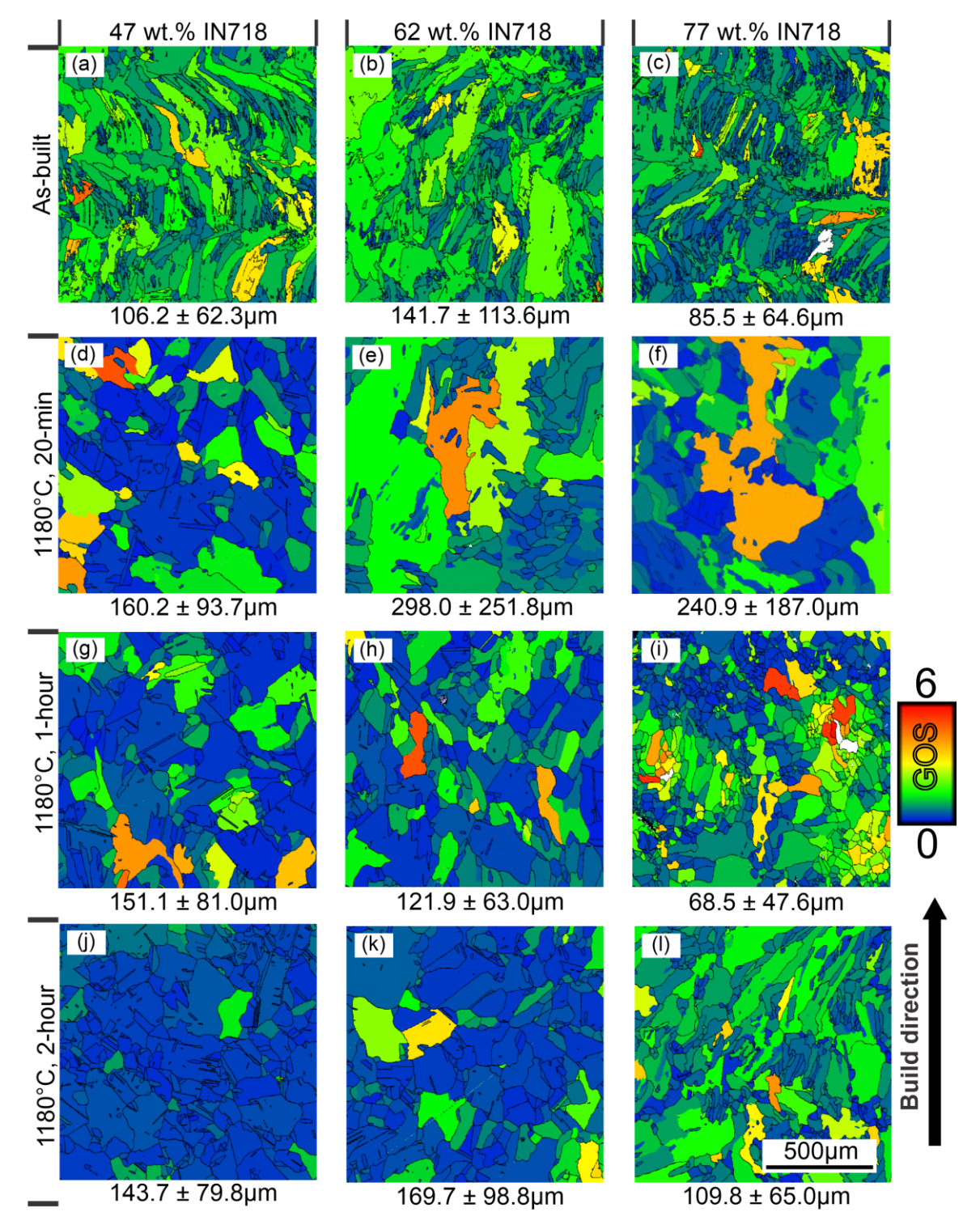


Figure 6. Grain orientation spread (GOS) maps of as-built and homogenized SS316-IN718 mixed alloys. GOS maps of mixed alloys under (a-c) as-built condition, after homogenization at 1180°C for (d-f) 20 mins, (g-i) 1 hour, and (j-l) 2 hours. The average grain size and standard deviation of each GOS map is shown below the image. The scale bar shown in (l) can also be used for the other microstructure images.

IN718, shown in Fig. 6(1), is still higher after 2-hour homogenization than the other two alloys.

4. Discussion

The entropy effects are intrinsic since they vary as a function of alloy composition. These three alloys are good candidates for deducing the effect of entropy on microstructure evolution because they all have similar phase stability, e.g., the same FCC matrix phase, similar amounts of the Laves phase in the as-built microstructure, and a similar small fraction of MC carbides. Additionally, all three alloys share a similar processing window. As shown in Fig. 1(e), these alloys exhibit different entropies. To evaluate the entropic impact on diffusion kinetics, Thermo-Calc software based on the thermodynamic TCNI11 database coupled with the mobility MOBNI5 database were used to estimate the diffusivities in each of the three alloy mixtures by calculating the diffusion matrix, as given in the **supplementary materials**. Close inspection of the diffusion matrix shows that most diffusivities decrease with increasing configurational entropy. However, if we assume that the diffusion process will be driven by the slowest diffusion, the alloy with 47 wt.% IN718 exhibits the slowest diffusion instead of 77 wt.% IN718, although the difference among these smallest diffusivities is rather negligible. Overall, the experimental observation and modeling above cannot provide strong evidence for a definitive relationship between grain kinetics and entropy. Although the initial experimental design was intended to reveal such a relationship, the debate regarding the influence of entropy on the diffusion kinetics in high-entropy alloy systems continues [29, 30].

One possibility is that the grain refinement from recrystallization is too strong, hiding the impact of entropy. Therefore, further work is required to quantitatively describe the effect of entropy on grain refinement and recrystallization in AM alloys. Consequently, it is more conclusive that in the alloy mixtures of SS316L and IN718, grain refinement observed during homogenization at 1180°C can be attributed to recrystallization, which is primary influenced by residual stress due to the complex heating and cooling cycles during the laser melting process. Even though such a strong influence of the residual stress and its dissipation through recrystallization could be the main cause for such a grain refinement, it is rather challenging to perform a quantitative analysis without reliable numerical simulations. Analysis of the grain size within each of the three alloys using EBSD reveals that the alloy mixture with the highest configurational entropy, 77 wt.% IN718, has the smallest grain size in the as-built condition and after homogenization for 1 hour at 1180°C.

5. Conclusions

- The capability of DED to fabricate alloys with different compositions by easily manipulating feedstock
 materials can accelerate alloy discovery and facilitate efficient studies of fundamental processmicrostructure-property relationships.
- By adding 77 wt.% IN718 to SS316L, a new alloy with a refined as-built microstructure is discovered. This fine grain structure exists even after high-temperature homogenization, and it was less pronounced in the other alloy mixtures with 47 and 62 wt.% IN718.
- There are three possible factors contributing to the grain refinement identified in this alloy: grain boundary pinning particles due to MC carbide formation, residual stress induced stored energy due to the unique laser melting process, and entropic influence on diffusion kinetics. More work is required to quantitatively identify these three factors and their role in grain structure evolution.
- It is reasonable to believe that high stored energy due to residual stress from the AM process plays a vital role in grain refinement by promoting recrystallization. Both entropy and grain boundary pinning effects may also contribute to the grain refinement observed in the studied samples. However, a more detailed mechanistic investigation is required.
- This work demonstrates a successful case study developing a new alloy by in-situ mixing of commercial feedstock powder, SS316L and IN718. The unique grain refinement observed during high-temperature homogenization indicates that the microstructure engineering of new alloys for additive manufacturing requires a comprehensive design and analysis in both as-printed and heat-treated conditions.

Declaration of Competing Interests

The authors declare that they have no known competing financial interests or personal relationships that could have appeared to influence the work reported in this paper.

Acknowledgments

W.X. acknowledges funding from the National Science Foundation under Faculty Early Career Development Award: CMMI 2047218. N.S. is supported by a NASA Space Technology Research Fellowship, Grant: 80NSSC19K1142.

References

- [1] D. Herzog, V. Seyda, E. Wycisk, C. Emmelmann, Additive manufacturing of metals, Acta Materialia 117 (2016) 371-392, doi:10.1016/j.actamat.2016.07.019.
- [2] T. DebRoy, H.L. Wei, J.S. Zuback, T. Mukherjee, J.W. Elmer, J.O. Milewski, A.M. Beese, A. Wilson-Heid, A. De, W. Zhang, Additive manufacturing of metallic components Process, structure and properties, Progress in Materials Science 92 (2018) 112-224, doi:10.1016/j.pmatsci.2017.10.001.
- [3] A. Ramakrishnan, G.P. Dinda, Microstructure and mechanical properties of direct laser metal deposited Haynes 282 superalloy, Materials Science and Engineering: A 748 (2019) 347-356, doi:10.1016/j.msea.2019.01.101.
- [4] Y. Zhao, K. Li, M. Gargani, W. Xiong, A comparative analysis of Inconel 718 made by additive manufacturing and suction casting: Microstructure evolution in homogenization, Additive Manufacturing 36 (2020) 101404, doi:10.1016/j.addma.2020.101404.
- [5] Y. Zhao, F. Meng, C. Liu, S. Tan, W. Xiong, Impact of homogenization on microstructure-property relationships of Inconel 718 alloy prepared by laser powder bed fusion, Materials Science and Engineering: A 826 (2021) 141973, doi:10.1016/j.msea.2021.141973.
- [6] A. Singh, S. Kapil, M. Das, A comprehensive review of the methods and mechanisms for powder feedstock handling in directed energy deposition, Additive Manufacturing 35 (2020) 101388, doi:10.1016/j.addma.2020.101388.
- [7] A. Reichardt, Additive Manufacturing of Metal-Based Functionally Graded Materials, University of California, Berkeley, Ann Arbor, 2017, p. 237,
- [8] A. Reichardt, A.A. Shapiro, R. Otis, R.P. Dillon, J.P. Borgonia, B.W. McEnerney, P. Hosemann, A.M. Beese, Advances in additive manufacturing of metal-based functionally graded materials, International Materials Reviews 66(1) (2020) 1-29, doi:10.1080/09506608.2019.1709354.
- [9] D.C. Hofmann, J. Kolodziejska, S. Roberts, R. Otis, R.P. Dillon, J.-O. Suh, Z.-K. Liu, J.-P. Borgonia, Compositionally graded metals: A new frontier of additive manufacturing, Journal of Materials Research 29(17) (2014) 1899-1910, doi:10.1557/jmr.2014.208.
- [10] W. Xiong, Additive manufacturing as a tool for high-throughput experimentation, Journal of Materials Informatics 2(3) (2022) 12, doi:10.20517/jmi.2022.19.
- [11] B.A. Welk, M.A. Gibson, H.L. Fraser, A combinatorial approach to the investigation of metal systems that form both bulk metallic glasses and high entropy alloys, JOM 68(3) (2016) 1021-1026, doi:10.1007/s11837-015-1779-8.
- [12] D. Kong, C. Dong, X. Ni, L. Zhang, C. Man, J. Yao, Y. Ji, Y. Ying, K. Xiao, X. Cheng, X. Li, High-throughput fabrication of nickel-based alloys with different Nb contents via a dual-feed additive manufacturing system: Effect of Nb content on microstructural and mechanical properties, Journal of Alloys and Compounds 785 (2019) 826-837, doi:10.1016/j.jallcom.2019.01.263.
- [13] J.W. Pegues, M.A. Melia, R. Puckett, S.R. Whetten, N. Argibay, A.B. Kustas, Exploring additive manufacturing as a high-throughput screening tool for multiphase high entropy alloys, Additive Manufacturing 37 (2021) 101598, doi: 10.1016/j.addma.2020.101598.
- [14] J.A. Glerum, C. Kenel, T. Sun, D.C. Dunand, Synthesis of precipitation-strengthened Al-Sc, Al-Zr and Al-Sc-Zr alloys via selective laser melting of elemental powder blends, Additive Manufacturing 36 (2020) 101461, doi:10.1016/j.addma.2020.101461.
- [15] Y. Chen, X. Zhang, M.M. Parvez, F. Liou, A Review on Metallic Alloys Fabrication Using Elemental Powder Blends by Laser Powder Directed Energy Deposition Process, Materials, 13(16) (2020) 3562, doi:10.3390/ma13163562.
- [16] M. Moorehead, K. Bertsch, M. Niezgoda, C. Parkin, M. Elbakhshwan, K. Sridharan, C. Zhang, D. Thoma, A. Couet, High-throughput synthesis of Mo-Nb-Ta-W high-entropy alloys via additive manufacturing, Materials & Design 187 (2020) 108358, doi:10.1016/j.matdes.2019.108358.

- [17] C. Wang, X.P. Tan, Z. Du, S. Chandra, Z. Sun, C.W.J. Lim, S.B. Tor, C.S. Lim, C.H. Wong, Additive manufacturing of NiTi shape memory alloys using pre-mixed powders, Journal of Materials Processing Technology 271 (2019) 152-161, doi:10.1016/j.jmatprotec.2019.03.025.
- [18] A. Aversa, G. Marchese, E. Bassini, Directed Energy Deposition of AISI 316L Stainless Steel Powder: Effect of Process Parameters, Metals 11(6) (2021) 932, doi:10.3390/met11060932.
- [19] J. Wanni, J.G. Michopoulos, A. Achuthan, Influence of cellular subgrain feature on mechanical deformation and properties of directed energy deposited stainless steel 316 L, Additive Manufacturing 51 (2022) 102603, doi:10.1016/j.addma.2022.102603.
- [20] R. Ghanavati, H. Naffakh-Moosavy, M. Moradi, Additive manufacturing of thin-walled SS316L-IN718 functionally graded materials by direct laser metal deposition, Journal of Materials Research and Technology 15 (2021) 2673-2685, doi:10.1016/j.jmrt.2021.09.061.
- [21] X. Ni, D. Kong, W. Wu, L. Zhang, C. Dong, Deformation-induced martensitic transformation in 316L stainless steels fabricated by laser powder bed fusion, Materials Letters 302 (2021) 130377, doi:10.1016/j.matlet.2021.130377.
- [22] W.-S. Shin, B. Son, W. Song, H. Sohn, H. Jang, Y.-J. Kim, C. Park, Heat treatment effect on the microstructure, mechanical properties, and wear behaviors of stainless steel 316L prepared via selective laser melting, Materials Science and Engineering: A 806 (2021) 140805, doi:10.1016/j.msea.2021.140805.
- [23] N. Sargent, M. Jones, R. Otis, A.A. Shapiro, J.-P. Delplanque, W. Xiong, Integration of Processing and Microstructure Models for Non-Equilibrium Solidification in Additive Manufacturing, Metals 11(4) (2021) 570, doi:10.3390/met11040570.
- [24] X. Wang, X. Gong, K. Chou, Review on powder-bed laser additive manufacturing of Inconel 718 parts, Proceedings of the Institution of Mechanical Engineers, Part B: Journal of Engineering Manufacture 231(11) (2016) 1890-1903, doi:10.1177/0954405415619883.
- [25] S.H. Kim, H. Lee, S.M. Yeon, C. Aranas, K. Choi, J. Yoon, S.W. Yang, H. Lee, Selective compositional range exclusion via directed energy deposition to produce a defect-free Inconel 718/SS 316L functionally graded material, Additive Manufacturing 47 (2021) 102288, doi:10.1016/j.addma.2021.102288.
- [26] E. Chikarakara, S. Naher, D. Brabazon, Spinodal decomposition in AISI 316L stainless steel via high-speed laser remelting, Applied Surface Science 302 (2014) 318-321, doi:10.1016/j.apsusc.2013.10.099.
- [27] K. Li, J. Zhan, P. Jin, Q. Tang, D.Z. Zhang, W. Xiong, H. Cao, Functionally Graded Alloys from 316 Stainless Steel to Inconel 718 by Powder-Based Laser Direct Energy Deposition, TMS 2022 151st Annual Meeting & Exhibition Supplemental Proceedings, Springer International Publishing, Cham, 2022, pp. 304-312, doi:10.1007/978-3-030-92381-5 28.
- [28] K. Li, X. Wang, W. Xiong, Functionally Graded Material Fabricated by Powder-based Laser Directed Energy Deposition: From Conventional to Complex Concentrated Alloys, Preprints 2022040139 (2022), doi:10.20944/preprints202204.0139.v1.
- [29] T. Koyama, Y. Tsukada, T. Abe, Simple Approach for Evaluating the Possibility of Sluggish Diffusion in High-Entropy Alloys, Journal of Phase Equilibria and Diffusion 210 (2022) 68–77, doi:10.1007/s11669-022-00938-9.
- [30] K. Biswas, J.-W. Yeh, P.P. Bhattacharjee, J.T.M. DeHosson, High entropy alloys: Key issues under passionate debate, Scripta Materialia 188 (2020) 54-58, doi:10.1016/j.scriptamat.2020.07.010.
- [31] J.O. Andersson, T. Helander, L. Höglund, P. Shi, B. Sundman, Thermo-Calc & DICTRA, computational tools for materials science, Calphad 26(2) (2002) 273-312, doi:10.1016/S0364-5916(02)00037-8.
- [32] D. Field, L. Bradford, M. Nowell, T. Lillo, The role of annealing twins during recrystallization of Cu, Acta Materialia 55 (2007) 4233-4241, doi:10.1016/j.actamat.2007.03.021.